

GNSS airborne multipath errors distribution using the high resolution aeronautical channel model and comparison to SARPs error curve

Christophe Macabiau, Laetitia Moriella, Mathieu Raimondi, Cyril Dupouy, A Steingass, A Lehner

▶ **To cite this version:**

Christophe Macabiau, Laetitia Moriella, Mathieu Raimondi, Cyril Dupouy, A Steingass, et al.. GNSS airborne multipath errors distribution using the high resolution aeronautical channel model and comparison to SARPs error curve. ION NTM 2006, National Technical Meeting of The Institute of Navigation, Jan 2006, Monterey, United States. pp 454 - 467. hal-01021775

HAL Id: hal-01021775
https://enac.hal.science/hal-01021775

Submitted on 29 Oct 2014

HAL is a multi-disciplinary open access archive for the deposit and dissemination of scientific research documents, whether they are published or not. The documents may come from teaching and research institutions in France or abroad, or from public or private research centers.

L'archive ouverte pluridisciplinaire **HAL**, est destinée au dépôt et à la diffusion de documents scientifiques de niveau recherche, publiés ou non, émanant des établissements d'enseignement et de recherche français ou étrangers, des laboratoires publics ou privés.

GNSS Airborne Multipath Errors Distribution Using the High Resolution Aeronautical Channel Model and Comparison to SARPs Error Curve

Christophe Macabiau, Laetitia Moriella, Mathieu Raimondi, *ENAC*
Cyril Dupouy, *STNA*
Alexander Steingass, Andreas Lehner, *DLR*

BIOGRAPHY

Christophe Macabiau graduated as an electronics engineer in 1992 from ENAC (Ecole Nationale de l'Aviation Civile) in Toulouse, France. Since 1994, he has been working on the application of satellite navigation techniques to civil aviation. He received his Ph.D. in 1997 and has been in charge of the signal processing lab of the ENAC since 2000.

Laetitia Moriella will graduate in 2006 as an electronics engineer from the Ecole Nationale de l'Aviation Civile (ENAC) in Toulouse, France.

Mathieu Raimondi graduated in 2005 as an electronics engineer from the Ecole Nationale de l'Aviation Civile (ENAC) in Toulouse, France. He is currently a Ph.D. student involved in the ANASTASIA project.

Cyril Dupouy has been working for STNA as a consultant engineer in GNSS since 1994. He graduated as an engineer in Aeronautics from the French National School of Civil Aviation (ENAC) in 1993. After initially being involved in a number of GNSS experiments and studies for STNA, he joined in 1998 the New Landing Systems division where he was in charge of GBAS studies and the certification process of GBAS ground equipment.

Alexander Steingass was born in Mettmann, Germany in 1969. He received his Dipl. Ing. Diploma in Electrical Engineering in 1997 (University of Ulm, Germany). Since then he has been a research scientist at the German Aerospace Centre DLR - Institute of Communications and Navigation. He has been involved in several projects in the area of satellite navigation and location dependent mobile services. In 2002 he was promoted Dr. Ing. at the University of Essen.
Homepage: http://www.dlr.de/kn/kn-s/steingass
Email: alexander.steingass@dlr.de

Andreas Lehner was born in Gmunden, Austria in 1973. He received his diploma engineer degree in mechatronics from the University of Linz in 2001. Since then he has been a research scientist at the German Aerospace centre DLR.
Homepage: http://www.dlr.de/kn/kn-s/lehner
Email: andreas.lehner@dlr.de

ABSTRACT

Because of its coverage, GNSS is a very attractive mean to provide the navigation service at every stage of the flight of an aircraft. In this purpose, the proposed system must comply with ICAO requirements, which include accuracy and integrity requirements. For example, during the approach, the position is highly critical information. The system performance during this phase of flight can be guaranteed through mitigation of the error sources and through a reliable estimation of their characteristics to protect the users by delivering appropriate integrity bounds.

In the studied case, we are interested in multipath during aircraft approaches. Indeed, the sum of direct and reflected signals induces a biased measurement affecting the reported position along the approach path. This bias may not be very large, but it needs to be appropriately taken into account in the error budget. Hence, it would be interesting to compute the statistics of the error due to multipath so as to predict adequately the measurement error standard deviation and then protect the user through pertinent integrity bounds.

This work was already tackled by RTCA for GPS L1 C/A code users, and the final result was a standard curve adopted in the ICAO SARPs stating the standard deviation of the error due to multipath as a function of the GPS satellite elevation angle. In the framework of the European ANASTASIA project, which aims at carrying out research, evaluation and cost benefit analysis of communication and navigation new technologies, the characteristics of the error induced by multipath needs to be determined for an aircraft using new GNSS signals transmitted by future GPS and GALILEO constellations.

In this purpose, it was decided to use an aeronautical channel model developed for ESA, coupled to a generic receiver simulator. The channel model was developed as a result of a measurement campaign carried out in 2002 by DLR, Joanneum Research, and the University of Vigo for ESA. Two planes were used, one as a transmitter and the second as a receiver. The second one was performing a landing procedure. Then, a model called ´high resolution aeronautical multipath navigation channel´ was designed.

This model completely describes the aeronautical channel and calculates the characteristics of the received signal. It is assumed to be composed of a direct ray, and reflected rays from different sources. The model separates the reflected rays in two different kinds: fuselage and ground echo. The parameters used in the implemented channel model were determined thanks to the measurement campaign.

The last investigated point is the terrain dependence. As explained above, the parameters of the model were determined thanks to the measurements, so it is likely that those parameters are not suitable for any other airport, particularly the ground reflection. This means that each airport will have its own parameters. As performing a measurement campaign on each and every airport is not bearable, the validity of these results need to for any airport needs to be investigated.

The aim of this paper is therefore to present the estimated standard deviation of the error due to multipath for a landing aircraft using any new GNSS signal. This estimation is provided by the overall conjunction of the aeronautical channel model and our GNSS receiver simulator.

1. INTRODUCTION

The main errors affecting the pseudorange measurements made by an aircraft during a final approach are due to the ionosphere, multipath, interference troposphere and noise.

One of the tasks of the ANASTASIA project is to characterize the threat represented by multipath during the final approach for future GNSS receivers, tracking future GPS and GALILEO signals.

A similar work had been conducted within RTCA years ago for GBAS and SBAS differential GPS L1 C/A code users [Booth et al., 2000]. The main result had been a curve representing the standard deviation of the smoothed tracking errors due to multipath as a function of the satellite elevation, adopted by ICAO.

To complete that task, it was agreed to use the High Resolution Aeronautical channel model developed for ESA [Steingass et al., 2004], and inject the output multipath parameters into a software receiver simulating the tracking process for the future GNSS signals.

This multipath model is provided as a Matlab software package by DLR, and we used it as an input of a GNSS receiver simulator, comprising code and phase tracking loops fed by correlator outputs affected by the multipath signals predicted by the channel model. We ran several simulations along the same path in order to compute statistics about the error due to multipath depending on the elevation. The model allows to compute multipath parameters and so the involved error. It is then compared to the ICAO SARPs curve for multipath standard deviation contribution. Those results are shown for different receiver configurations (correlator width, filter bandwidth, etc.), and the influence of ground and fuselage reflections are compared.

The aim of this paper is therefore to present the estimated standard deviation of the error due to multipath for a landing aircraft using any new GNSS signal. This estimation is provided through simulation by the overall conjunction of the aeronautical channel model and our GNSS receiver simulator.

The paper is organized as follows: first we present the ICAO multipath model for GPS L1 C/A. Then the model designed from measurement at Graz Airport will be depicted. Our generic GNSS receiver simulator is then presented. Then, the modeled multipath errors standard deviation will be presented for all GNSS signals, and contribution of each signal and receiver feature will be described. Finally, tests on the validity of the ground reflection power are presented.

2. SARPs ERROR CURVE

As stated in [Booth et al., 2000], an airborne pseudorange accuracy allocation for differential GPS L1 C/A systems was determined by RTCA. That allocation includes the contribution of the airborne receiver thermal noise and the airborne multipath. A standard model for the standard deviation of the airborne multipath was developed and validated. The assumed sigma value is specified to be included in the term used in the weighting matrix for the position solution and in the Protection Level equations.

The adopted sigma model was proposed in [Murphy and Booth, 1999] and [Murphy and Booth, 2000], and validated from efforts made by the FAA, Boeing and Honeywell, mainly using data collected for years during normal production flight testing. Through this joint activity, the data from 6 different models of Boeing airplanes were collected and analyzed.

The paper [Booth et al., 2000] presents information regarding the work that has been done to validate the standard multipath error expression. The authors also stress the difficulty to assess the tails of the distribution of the multipath errors.

The study appeared to indicate that the distribution of airframe multipath errors does depend on the specific airframe, but that the distributions are similar enough that a single curve may adequately cover all airframes.

The adopted curve has the following expression, plotted in figure 1:

$$\sigma = 0.13 + 0.53 \times \exp\left(-\theta_{\deg}/10\right) \text{ in meters.}$$

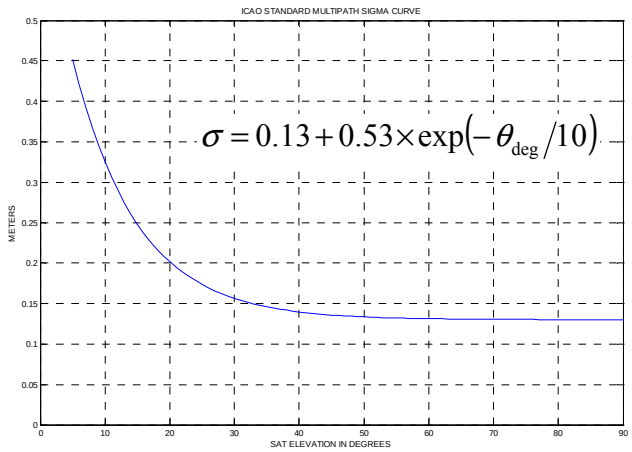


Figure 1: *ICAO airbone multipath sigma curve for differential GPS L1 C/A systems.*

Recently, a new measurement campaign was conducted in order to refine this curve [Murphy et al., 2005a], [Murphy et al., 2005b]. Indeed, it is believed that this curve took into account other error sources than rather just multipath, and thus a new campaign was launched to check that curve. Among the objectives, it was interesting to check whether it is necessary to define separate models for the airframe and ground multipath.

As stated by the authors, the new flight test data seem to indicate that the current airborne multipath model is a reasonable (if slightly conservative) representation of the airframe and ground bounce multipath.

It is believed by the authors in [Murphy et al., 2005b] that their electromagnetic model results are probably a more accurate estimate of the true code phase multipath errors. Consequently, these authors think it should be possible to consider a somewhat tighter model.

In addition, the new campaign seems to indicate that the ground echo has a negligible influence on the result.

3. HIGH RESOLUTION AERONAUTICAL CHANNEL MODEL

Along with the development of GALILEO it became necessary to improve the knowledge about the aeronautical channel. Especially the power, the origin and the delay of the reflections at the aircraft structure were a main topic in the scientific discussions. During this exchange of opinions the lack of information concerning the bandwidth of the reflections became obvious. For that reason the European Space Agency (ESA) commissioned a contract about a measurement campaign on this issue in autumn 2002 to a research consortium, consisting of Joanneum Research (Austria), University of Vigo (Spain) and the German Aerospace Centre (Germany).

The results of the investigation carried out by this consortium were presented in [Steingass et al., 2004].

Measurement campaign

The channel characteristics were measured using a channel sounder during standard ILS approaches, and static measurements were made with the airplane on the ground.

The approaches were flown at Thalerhof airport of Graz, Austria using an ATTAS VFW 614. Another airplane was used as the transmitting platform of a signal at 1.95 GHz using a bandwidth of 100 MHz in order to measure the channel impulse response.

In a second step, a helicopter carrying the transmitter circled the ATTAS VFW 614 plane parked on the ground, while the reflections on the plane were measured. To allow an extension of the measurement results to larger aircrafts, the ground measurements were repeated with an Airbus A340.

The channel impulse response was observed in order to estimate the characteristics of the different multipath rays (time delay, amplitude...). Then, these observations were used to define the channel model.

Figure 2 is an illustration of the measurements made.

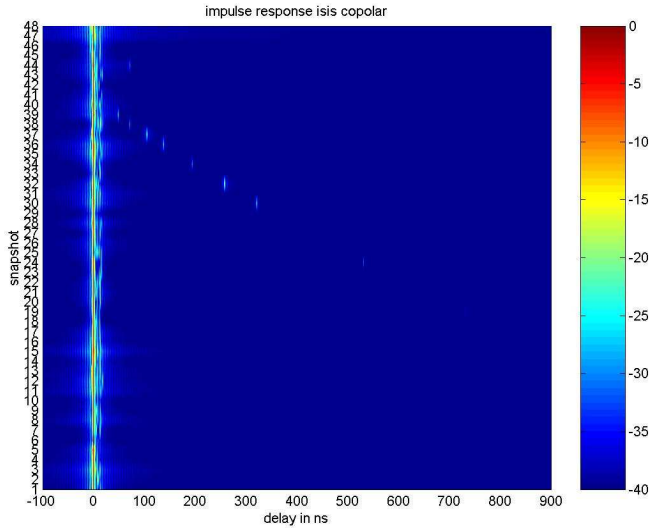


Figure 2: *Channel impulse response of the final approach in a large time scale.*

In figure 2, the Line-Of-Sight signal can be seen at 0 ns delay. The other points correspond to multipath: the reflected rays have a larger time delay with respect to the direct ray and have lower amplitude. The large delay points are related to ground reflection. This delay is dependent on the aircraft altitude and is varying between 900 and 10 ns. The ground reflection power is varying between the different flights but can be estimated in a range of -15 to -25 dB.

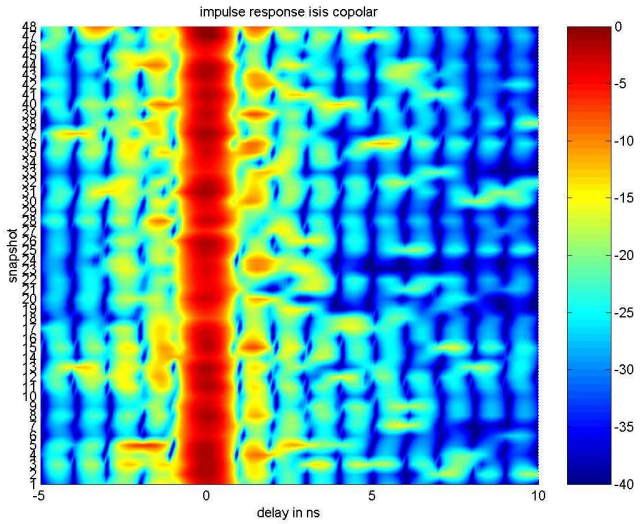


Figure 3: *Measured impulse response-short time scale.*

As we can see in figure 3, there is quite a strong reflection very close to the direct signal at approximately 1-2 ns delay with a certain modulation.

It has been located on the fuselage near the antenna and called the fuselage echo. The power of this echo is estimated to -14.2 dB. The measurements do not show any wing reflection.

The results of the measurement campaign show that multipath error is almost due to the fuselage echo and the ground reflection, and that a zero-delay replica is present, causing LOS signal fading and phase distortion.

Adopted model

From the results of the measurement campaign, it was decided that the model would be a direct path (Path 0), a refractive component of the direct path (Path 1), an strong echo on the fuselage that is changing very slowly (Path 2), and a quickly changing ground echo (Path3). The output states of the model will be the parameters of multipath: time delay, amplitude and phase.

We have seen in the precedent section that, from measurements, values of time delay and reflection power for each ray of their model were determined.

But, the evolution in time of multipath parameters needs to be taken into account. That's why simulations were made by using the recorded pitch, yaw and roll flight data to estimate the power spectrum.

The ground echo is modulated by the reflecting terrain structure. That's why the approach is divided into three different zones of altitude (high, mid and low altitude) in order to characterise the ground reflection which is characterized in each zone by a Markov state. The Markov model described here is specific at Graz airport.

The Markov parameters are the vector of the power values, and the transition matrix P containing the probability of changing from each power state determined for each altitude region independently.

The delay of the ground reflection depends on the altitude of the airplane and the elevation angle of the satellite as $d = 2 \cdot h \cdot \sin(\theta)$.

The fading processes have input parameters dependent on satellite elevation and azimuth.

The complete aeronautical channel model is shown in figure 4.

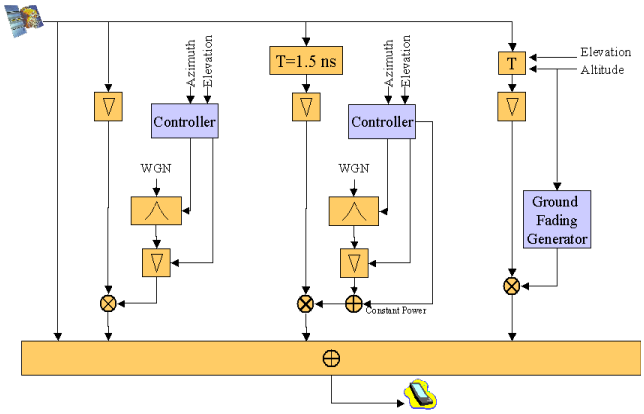


Figure 4: *Complete aeronautical channel model.*

The first branch is the direct signal, followed by the refractive part modelling the modulation. The third branch models the fuselage echo and the last branch is the ground echo.

Examples of outputs

The Matlab files implementing this channel model and provided for download on DLR web site http://www.kn-s.dlr.de/satnav are used in this application for an aircraft flying a typical approach with an altitude profile as shown in figure 5. The simulation interval is 500s, including a first 300s segment with an altitude descending rate of 0.5 m/s, followed by a 200s segment with a descending rate of 3.8 m/s. This profile simulates a generic A340 GNSS approach procedure.

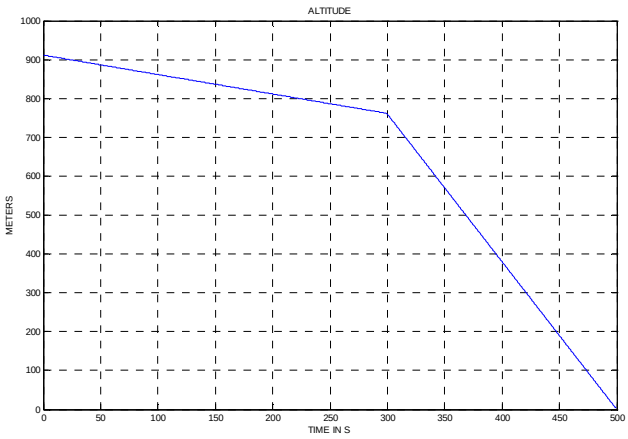


Figure 5: *Aircraft altitude profile.*

With such an altitude profile, the High Resolution Aeronautical channel model is used to deliver ground and fuselage echo characteristics such as relative

amplitude α, phase $\Delta\theta$ and delay $\Delta\tau$ w.r.t. the L.O.S. ray for an A340. The satellite elevation angle is assumed to be constant during the approach, as during the 500 seconds the satellite elevation angle does not vary much. The default sampling rate for the output of the multipath parameters, used in this project, is set to Fs=25.4 Hz in the channel model Matlab files. Typical outputs for elevation angles of 10° and 70° are shown in the next figures.

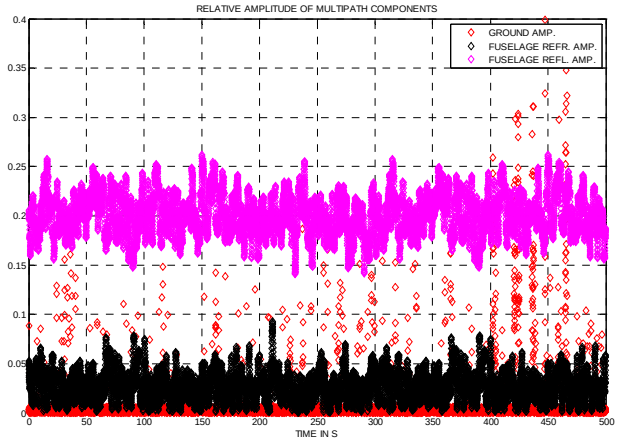


Figure 6: *Relative amplitude of multipath components for a satellite angle of 10° (A340).*

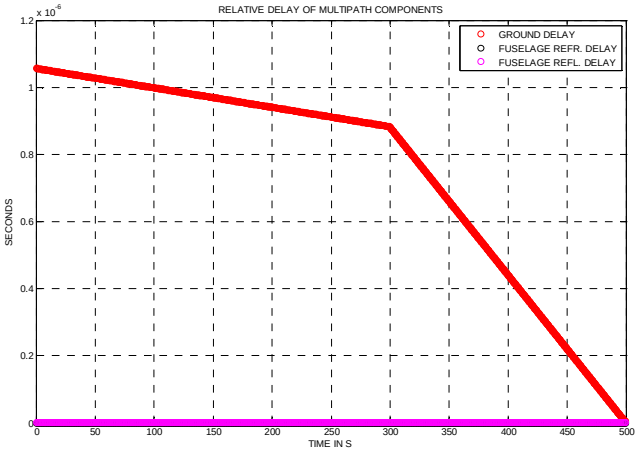


Figure 7: *Relative delay of multipath components for a satellite angle of 10° (A340).*

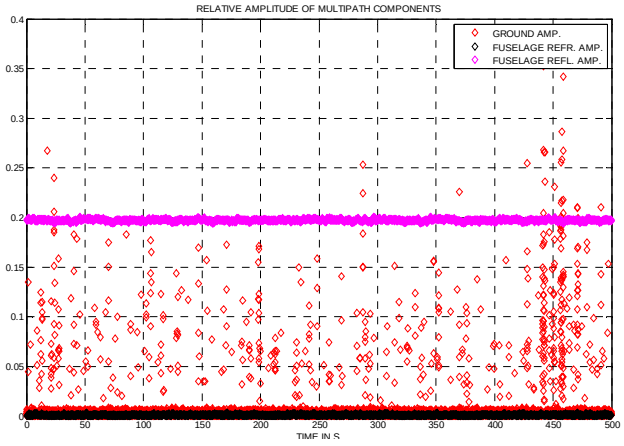


Figure 8: *Relative amplitude of multipath components for a satellite angle of 70° (A340).*

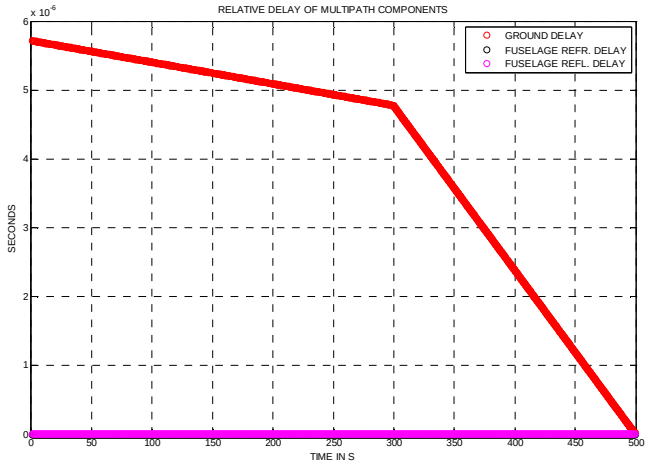


Figure 9: *Relative delay of multipath components for a satellite angle of 70° (A340).*

We can see in figures 6 and 8 that the relative amplitude of each 3 rays has distinct behaviours: the ground echo most of the time has very small amplitude, but sudden high peaks (up to 0.4) can be experienced. The fuselage reflection amplitude is around 0.2, and has more fluctuations for satellites at low elevation angles. The zero delay fuselage component has small amplitudes (lower than 0.05), and its amplitude decreases quite well when the sat elevation is increasing.

As we can see from figures 5, 7, 9, the delay of the ground reflection varies linearly as a function of the aircraft altitude. It is roughly within one microsecond during all the approach for a sat elevation angle of 10°, but at 70° the delay is larger and close to one microsecond only during the last 50s of the approach. Therefore, this ground reflection echo may have an influence only at low elevation angles for signals with a chip rate Fc=1.023 MHz (GPS and GALILEO L1), but negligible influence for high chip rate signals (GPS L5, GALILEO E5a/E5b) at high elevations. In addition as seen previously the amplitude variation of the ground echo is rapid, thus it behaves like noise. It is likely to be filtered out by the code-carrier smoothing filter. The delay of the fuselage echoes is very small, set to 1.5 ns and 0 s in the channel model as per the observations.

4. RECEIVER SIMULATOR IMPLEMENTATION

The multipath parameters generated by the High Resolution Aeronautical channel model are then used to generate the correlator outputs using the following model:

$$\begin{cases} I_p = \sum_{i=0}^{3} \alpha_i \cdot \widetilde{K}_c(\varepsilon_\tau + \Delta\tau_i) \cdot \cos(\varepsilon_\theta + \Delta\theta_i) \\ Q_p = \sum_{i=0}^{3} \alpha_i \cdot \widetilde{K}_c(\varepsilon_\tau + \Delta\tau_i) \cdot \sin(\varepsilon_\theta + \Delta\theta_i) \end{cases}$$

$$
\begin{cases}
I_E = \sum_{i=0}^{3} \alpha_i \cdot \tilde{K}_c(\varepsilon_\tau + C_S/2 + \Delta\tau_i) \cdot \cos(\varepsilon_\theta + \Delta\theta_i) \\
Q_E = \sum_{i=0}^{3} \alpha_i \cdot \tilde{K}_c(\varepsilon_\tau + C_S/2 + \Delta\tau_i) \cdot \sin(\varepsilon_\theta + \Delta\theta_i) \\
I_L = \sum_{i=0}^{3} \alpha_i \cdot \tilde{K}_c(\varepsilon_\tau - C_S/2 + \Delta\tau_i) \cdot \cos(\varepsilon_\theta + \Delta\theta_i) \\
Q_L = \sum_{i=0}^{3} \alpha_i \cdot \tilde{K}_c(\varepsilon_\tau - C_S/2 + \Delta\tau_i) \cdot \sin(\varepsilon_\theta + \Delta\theta_i)
\end{cases}
$$

where $\tilde{K}_c(\tau) = (h \otimes K_c)(\tau)$ is the filtered autocorrelation function of the PRN code. This filtered autocorrelation function is generated using the initial assumptions on the signal type (BPSK or BOC) and RF/IF filter characteristics (filter type and bandwidth).

Note that this model assumes the multipath parameters are constant during the integration interval.

The code and phase tracking loops implemented in the receiver simulator have the following parameters. The PLL is a 3rd order arctan loop with a bandwidth equal to 10 Hz. The DLL is coupled to the PLL and is a 1st order loop with a bandwidth equal to 1 Hz.

The DLL can have a dot-product or an Early-Minus-Late Power discriminator.

The correlator outputs are assumed to be affected by multipath only, we do not consider here the effect of noise

Figures 10 and 11 show examples of the code measurement errors observed in the receiver simulator when injecting a single reflected ray with a constant relative amplitude equal to 0.5 and a relative delay sweeping from 0 to 1.6 chip GPS C/A code chips.

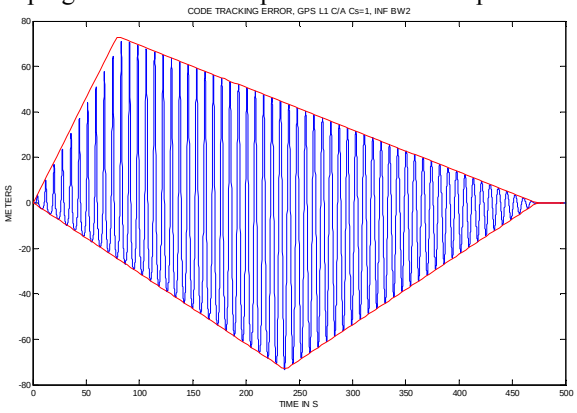


Figure 10: *Observed code tracking error plus theoretical envelope (BPSK, infinite bandwidth, wide correlator spacing Cs=1).*

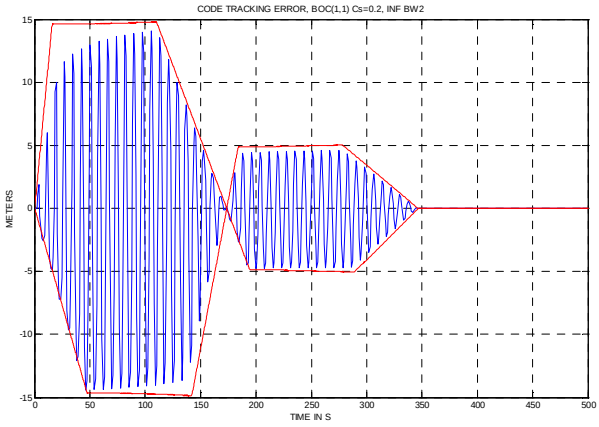


Figure 11: *Observed code tracking error plus theoretical envelope (BOC(1,1), infinite bandwidth, narrow correlator spacing Cs=0.2).*

As we can see in figures 10 and 11, the observed error fits within the theoretical error envelope, plotted with another tool.

5. SIMULATIONS CONFIGURATION

The High Resolution Aeronautical channel model and the receiver simulator are used together to provide an indication of what impact the multipath has on the pseudorange measurements made by a future GPS/GALILEO receiver onboard an aircraft flying a final approach.

To this end, the Matlab implementation of the High Resolution Aeronautical channel described in section 3 is run with the settings presented here. The assumed aircraft is an A340. The simulation interval is 500s. The input altitude profile is as presented in figure 15: it starts with a first 300s segment with an altitude descending rate of 0.5 m/s, followed by a 200s segment with a descending rate of 3.8 m/s. This profile simulates a generic A340 approach procedure. The parameters for the channel simulation are then left unchanged as in the original implementation.

The propagation channel is run 500 times per satellite elevation value, from 10° to 70° per 10° steps. That results in 7*500=3500 sets of multipath parameters, that are stored and then used identically for all the signal and tracking variations presented below. Thus, all signals and tracking options are tested against the same channel multipath configuration.

The receiver simulator, described in section 4, is run with the parameters presented here. For the results presented here, the DLL type is set to be a dot-product DLL.

The signal type is first set as BPSK, with Fc=1.023 MHz, as for GPS L1 C/A code. The bandwidth is set to BW2=2MHz, for a chip spacing Cs=1 chip. Then, for the same signal we set BW2=16MHz, for a chip spacing Cs=0.1 chip.

Then, we set Fc=10.23 MHz, as for GPS L5, GALILEO E5a and GALILEO E5b. The bandwidth is set to BW2=20MHz, for a chip spacing Cs=0.25 chip.

Finally, we set the signal type as BOC(1,1), with Fc=1.023 MHz as for GALILEO L1. The bandwidth is set to BW2=6MHz, for a chip spacing Cs=0.2 chip.

Then, the program stores the raw and 100s smoothed code and phase tracking errors at the end of the approach. Two independent samples are extracted from the smoothed code tracking error per approach. These two samples are taken separated by at least 200s, at random epochs in the interval [200s…460s-496s]. The first interval bound (200s) is chosen so as to eliminate samples where the code-carrier smoothing filter did not converge. The last interval bound depends on the lowest altitude considered for data analysis: 460s is the time at which the 500ft altitude is reached, 496s is the time at which the 50ft altitude is reached. Two types of results are presented here: statistics of code tracking error for an aircraft altitude higher than 500ft, statistics of code tracking error for an aircraft altitude higher than 0.

Examples of observed raw and smoothed code tracking errors are shown in figures 12, 13, 14, 15.

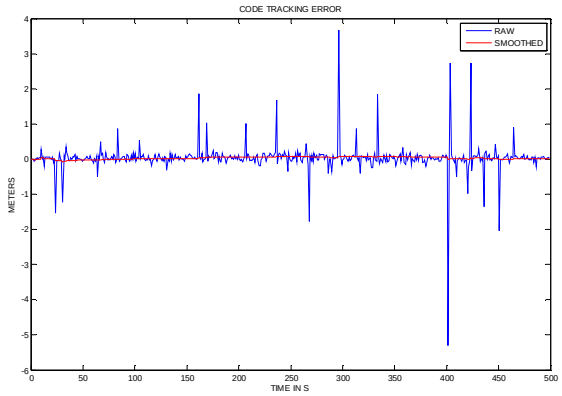


Figure 12: *Example simulated raw and smoothed code tracking error (GPS L1 C/A, BW2=2MHz, Cs=1, 10° sat).*

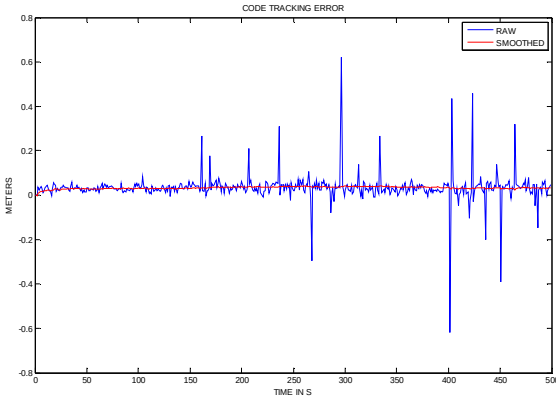


Figure 13: *Example simulated raw and smoothed code tracking error (GPS L1 C/A, BW2=16MHz, Cs=0.1, 10° sat).*

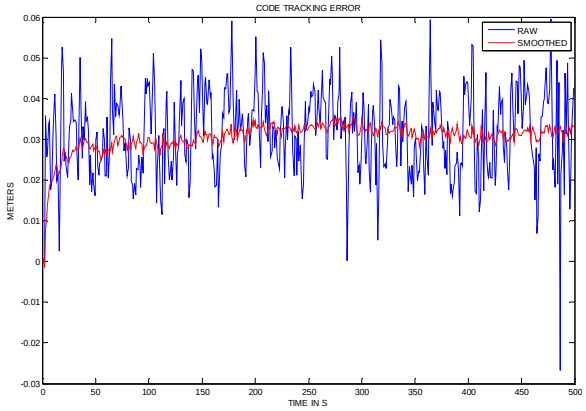


Figure 14: *Example simulated raw and smoothed code tracking error (GPS L5 GALILEO E5a/E5b, BW2=20MHz, Cs=0.25, 10° sat).*

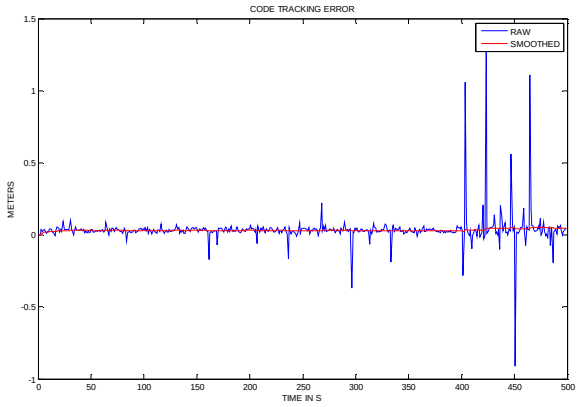


Figure 15: *Example simulated raw and smoothed code tracking error (GALILEO L1 BOC(1,1), BW2=6MHz, Cs=0.2, 10° sat).*

Figures 12,13,14,15 show the inherent resistance of each receiver configuration to the same multipath. The observed error is reduced from the GPS L1 C/A wide chip spacing receiver, to the BOC(1,1), narrow correlator and high chipping rate signal.

6. VALIDITY: RESULTS FOR GPS L1 C/A

The following simulations have been made with GPS L1 C/A code (FC=1.023 MHz) to compare the results with the ICAO SARPs curve.

Figure 16 shows the estimated standard deviation for a double sided bandwidth BW_2=2 MHz, a chip spacing C_S=1, and tracking loops bandwidths such as B_{PLL}=10 Hz, B_{DLL}=1 Hz.

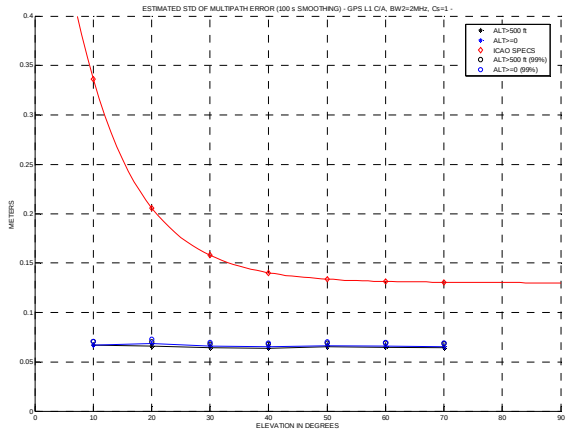


Figure 16: *Smoothed pseudorange error sigma compared to SARPS model (GPS L1 C/A, BW2=2 MHz, C_S=1 chip, 500 approaches per sat elevation, A340).*

As we can see in figure 16, the resulting sigma is almost constant with elevation, between 6 cm and 7 cm, and is lower than SARPs curve. This is mostly explained by the fact that the ground echo does not contribute much to the final error, as it mostly behaves like a high frequency error. Using traditional confidence interval theory on estimated variance with unknown mean, 99% bounds are also plotted, taking into account the fact that only 1000 independent samples taken out of the simulator are considered for each elevation angle (2 independent samples per simulated approach).

Figure 17 shows the ratio between the standard deviation of the raw code tracking error and the standard deviation of the smoothed tracking error. This ratio is labeled here the code-carrier smoothing effectiveness factor, as in [Murphy and Booth, 2005b].

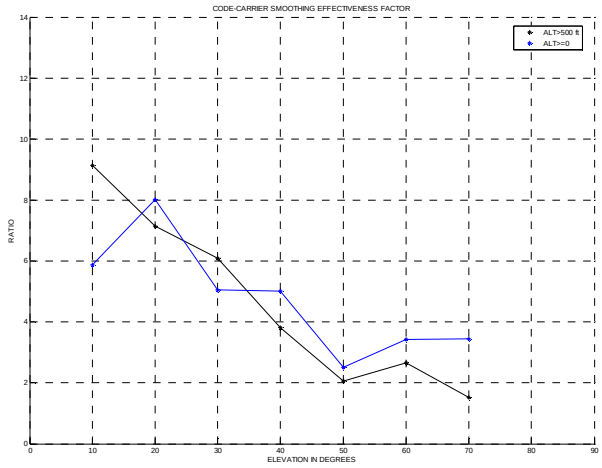


Figure 17: *Code-carrier smoothing effectiveness factor (GPS L1 C/A, BW2=2 MHz, C_S =1 chip, 500 approaches per sat elevation, A340).*

If the raw code tracking error was pure white noise, this ratio should be close to $10\sqrt{2} \approx 14.1$. We see in figure 18 that the observed ratio is close to 8 at 10°, and decreases to 3 at 70°. This result shows that the raw code tracking error due to multipath exhibits a very high correlation factor at high elevation angles, and resembles white noise at low elevation angles.

Figure 18 shows the observed distribution of the smoothed code tracking errors for satellite elevations 10° and 70°.

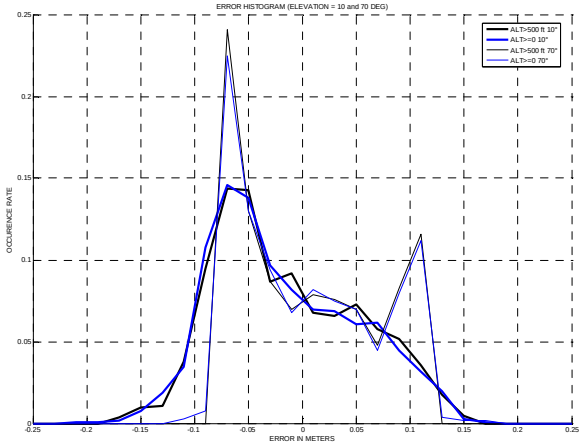


Figure 18: *Observed distribution of smoothed code tracking errors for elevations 10° and 70° (GPS L1 C/A, BW2=2 MHz, C_S =1 chip, ground reflection amplitude$\times 2$, 500 approaches per sat elevation, A340).*

As we can see in figure 18, the distribution lies roughly in [-0.2m…0.2m] at 10° and lies in [-0.1m…0.1m] at 70°. Also, this distribution does not look like a Gaussian distribution. For low elevation angles, such as 10°, the distribution is skewed, and therefore the tracking error has a small bias of 1.5 cm. At high elevation angles, the distribution resembles a uniform distribution, with peaks at both ends, still exhibiting a bias smaller than 4 mm.

As an illustration, figure 19 shows the unsmoothed code tracking error distribution.

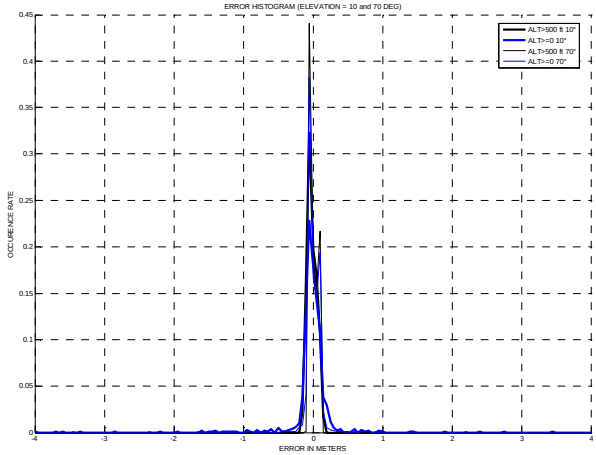


Figure 19: *Unsmoothed code tracking error distribution at 10° and 70° (GPS L1 C/A, BW2=2 MHz, C_S =1 chip, 500 approaches per sat elevation, A340).*

As we can see in figure 19, the unsmoothed code tracking errors are mostly distributed in [-0.3m…0.3m], but many large errors do exist.

Figure 20 shows the estimated standard deviation for a double sided bandwidth BW_2=2 MHz, C_S=1, B_PLL=10 Hz, B_DLL=1 Hz, no ground reflection:

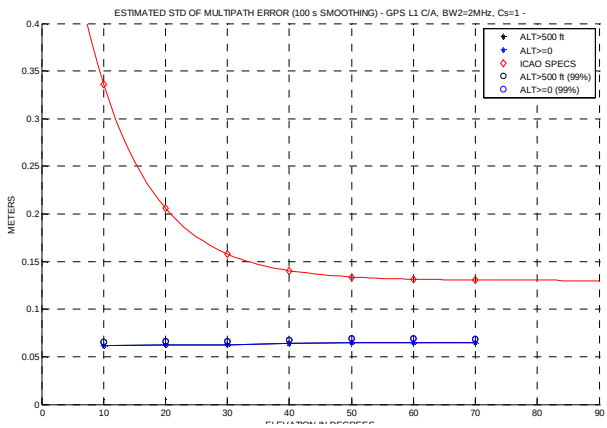


Figure 20: *Smoothed pseudorange error sigma compared to SARPS model (GPS L1 C/A, BW2=2 MHz, C_S =1 chip, no ground reflection, 500 approaches per sat elevation, A340).*

Resulting sigma is slightly smaller, still between 6 cm and 7 cm, similar to previous result with all multipath components, so ground reflection does not contribute much: the main contributor is the fuselage echo.

Figure 21 shows the code-carrier smoothing effectiveness factor in the case where no ground reflection is present.

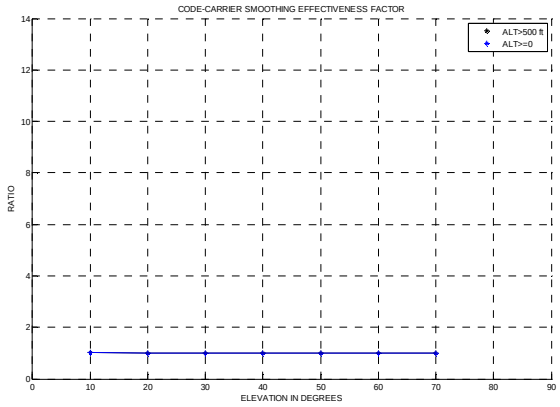


Figure 21: *Code-carrier smoothing effectiveness factor (GPS L1 C/A, BW2=2 MHz, C_S =1, no ground reflection, 500 approaches per sat elevation, A340).*

As we can see in figure 21, smoothing does not improve this error at all because it mostly has behaviour close to a bias in time for each run. This can also be seen in the error distribution, not shown here, that is very similar to the smoothed code error distribution, shown in figure 22.

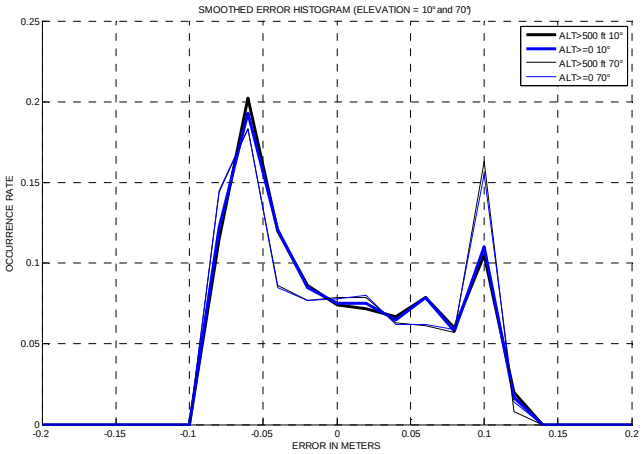


Figure 22: *Observed distribution of smoothed code tracking errors for elevations 10° and 70° (GPS L1 C/A, BW2=16 MHz, C_S =0.1 chip, no ground reflection, 500 approaches per sat elevation, A340).*

As we can see in figure 22, the distribution lies roughly in [-0.1m…0.15m]. This distribution does not look like a Gaussian distribution and resembles more a uniform distribution, with peaks at both ends, exhibiting a bias smaller than 4 mm.

Figure 23 shows the estimated standard deviation for a double sided bandwidth BW2=16 MHz, CS=0.1, B_PLL=10 Hz, B_DLL=1 Hz.

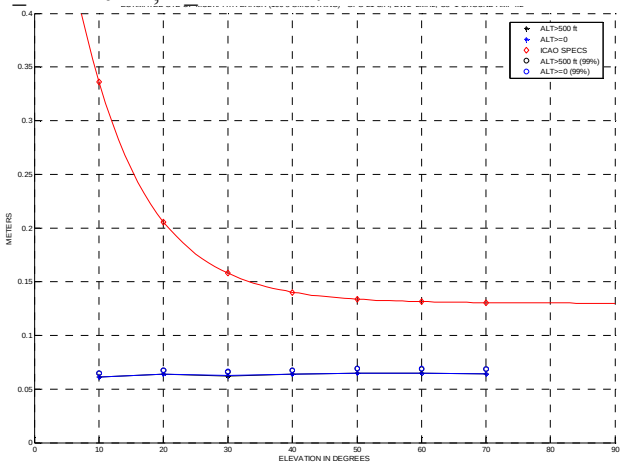


Figure 23: *Smoothed pseudorange error sigma compared to SARPS model (GPS L1 C/A, BW2=16 MHz, C_S =0.1 chip, 500 trials per elevation, A340).*

As we can see in figure 23, the resulting sigma is between 6 and 7 cm.

Figure 24 shows the code-carrier smoothing effectiveness factor.

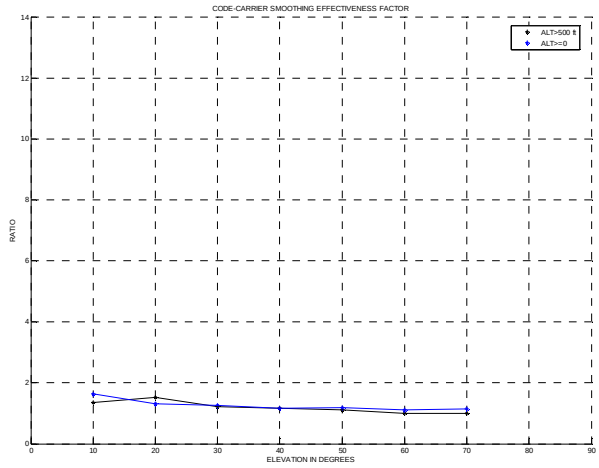


Figure 24: *Code-carrier smoothing effectiveness factor (GPS L1 C/A, BW2=16 MHz, C_S =0.1 chip, 500 approaches per sat elevation, A340).*

As we can see in figure 24, smoothing does not improve this error very much because it mostly has behaviour close to a bias in time for each run. This can also be seen in the unsmoothed error distribution, not shown here, that is very similar to the smoothed code error distribution.

7. RESULTS FOR L5, E5a, E5b

The following simulations have been made with GPS L5 or GALILEO E5a or GALILEO E5b code characteristics (F_C=10.23 MHz).

Figure 25 shows the estimated standard deviation for a double sided bandwidth BW_2=20 MHz, C_S=0.25, B_PLL=10 Hz, B_DLL=1 Hz.

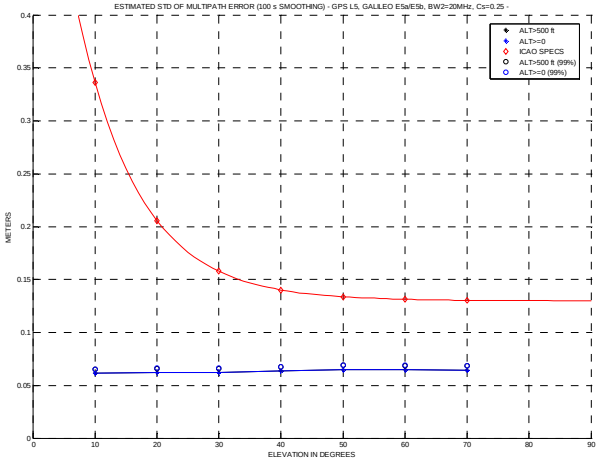


Figure 25: *Smoothed pseudorange error sigma compared to SARPS model (GPS L5, GALILEO E5a/E5b, BW2=20 MHz, B_PLL=10 Hz, B_DLL=1 Hz, C_S =0.25 chip, 500 approaches per sat elevation, A340).*

As we can see in figure 25, the estimated sigma is of the same size than for GPS L1 C/A code case, roughly constant between 6 and 7 cm. Other simulations made in that case with a reduced bandwidth BW2=16MHz and Cs=0.25, and generally with a narrow chip spacing did not show any noticeable change in the results.

Figure 26 shows the code-carrier smoothing effectiveness factor.

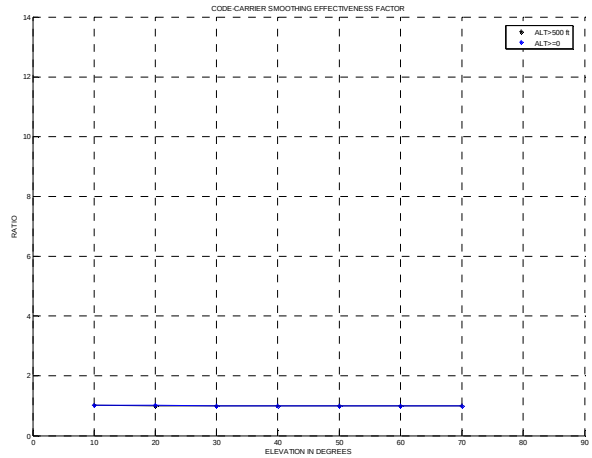


Figure 26: *Code-carrier smoothing effectiveness factor (GPS L5, GALILEO E5a/E5b, BW2=20 MHz, B_PLL=10 Hz, B_DLL=1 Hz, C_S =1 chip, 500 approaches per sat elevation, A340).*

As we can see in figure 26, smoothing does not improve this error at all because it mostly has a behaviour close to a bias in time for each run. This can also be seen in the unsmoothed code error distribution, not shown here, that is very similar to the smoothed code error distribution, shown in figure 27.

Figure 27 shows the smoothed pseudorange error distribution.

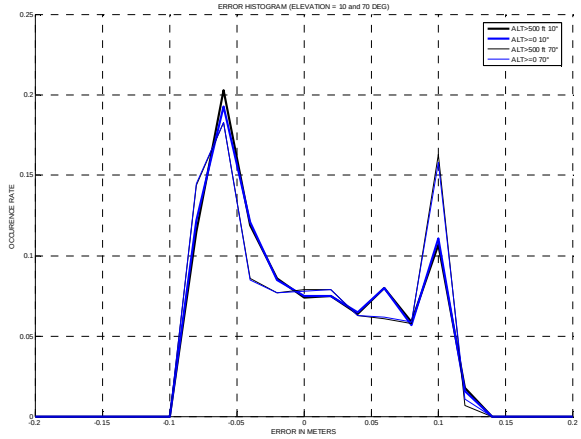


Figure 27: *Smoothed pseudorange error sigma compared to SARPS model (GPS L5, GALILEO E5a/E5b, BW2=20 MHz, B_PLL=10 Hz, B_DLL=1 Hz, C_S =0.25 chip, 500 approaches per sat elevation, A340).*

As we can see in figure 27, the distribution lies roughly in [-0.1m…0.15m]. This distribution does not look like a Gaussian distribution and resembles more a uniform distribution, with peaks at both ends, exhibiting a bias smaller than 3 mm.

8. RESULTS FOR GALILEO L1 BOC(1,1)

The following simulations have been made with GALILEO L1 BOC(1,1) signal characteristics (F_C=1.023 MHz, Fs=1.023 MHz).

Figure 28 shows the estimated standard deviation for a double sided bandwidth BW_2=6 MHz, C_S=0.2, B_PLL=10 Hz, B_DLL=1 Hz.

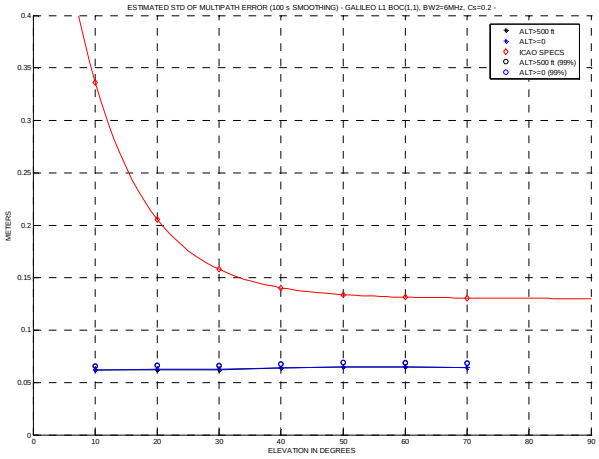


Figure 28: *Smoothed pseudorange error sigma compared to SARPS model (GALILEO BOC(1,1), BW2=6 MHz, B_PLL=10 Hz, B_DLL=1 Hz, C_S =0.2 chip, 500 approaches per sat elevation, A340).*

Resulting sigma is similar to GPS L1 C/A code case, as it is between 6 cm and 7 cm.

Figure 29 shows the code-carrier smoothing effectiveness factor for GALILEO L1 BOC(1,1), BW_2=6 MHz, C_S=0.2.

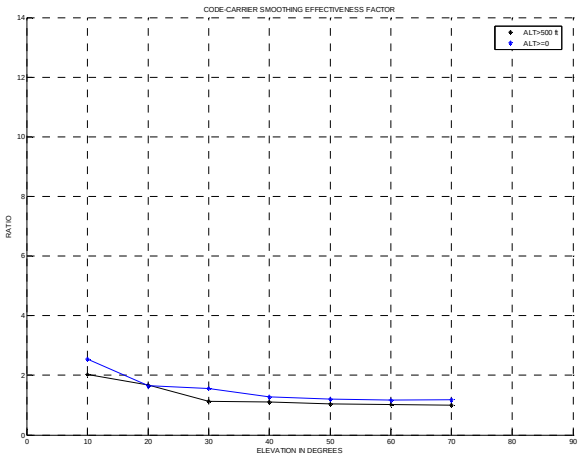


Figure 29: *Code-carrier smoothing effectiveness factor (GALILEO L1 BOC(1,1), BW2=6 MHz, C_S =0.2 chip, 500 approaches per sat elevation, A340).*

As we can see in figure 29, the smoothing effectiveness factor decreases as the elevation angle increases. But this factor is very small, only decreasing from 3 to 1. This means that the GALILEO BOC(1,1) tracking error reduction factor is quite limited, which is an indication that the error is highly correlated.

This is a general result already observed with large bandwidth and narrow correlator receivers during this study. That seems to reflect the fact that rapidly changing errors are eliminated by the receiver

Figure 30 shows the smoothed code error distribution for elevation angles 10° and 70°.

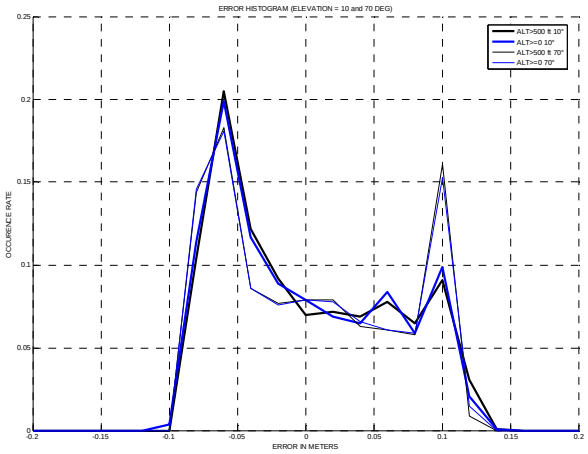


Figure 30: *Smoothed pseudorange error distribution for sat elevation angles 10° and 70° (GALILEO BOC(1,1), BW2=6 MHz, C_S =0.2 chip, 500 approaches per sat elevation, A340).*

As we can see in figure 30, the distribution of the smoothed code tracking errors lies roughly in [-0.1m…0.15m]. This distribution does not look like a Gaussian distribution and resembles more a uniform distribution, with peaks at both ends, exhibiting a bias smaller than 4 mm.

9. GROUND REFLECTION POWER ADAPTATION

In order to test the importance of the ground reflection power on the final estimated sigma, we have conducted several tests. The two main tests that were conducted consisted in multiplying the amplitude of the relative amplitude of the ground reflection by 2, and in amplifying it in such a way that the GPS L1 C/A estimated sigma curve matches roughly the standard L1 sigma curve.

Figure 31 shows the estimated standard deviation for a double sided bandwidth BW2=2 MHz, CS=1, B_PLL=10 Hz, B_DLL=1 Hz, amplitude of ground reflection multiplied by 2.

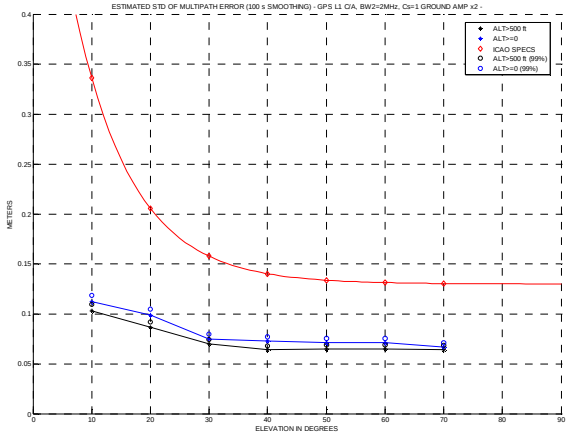


Figure 31: *Smoothed pseudorange error sigma compared to SARPS model (GPS L1 C/A, BW2=2 MHz,*

C_S =1 chip, ground reflection amplitude$\times 2$, 500 approaches per sat elevation, A340).

As we can see in figure 31, the resulting sigma is still lower than SARPs curve, but the observed value does increase at low elevation angles compared to figure 16 where the channel model is used with its initial settings. The maximum value is 12 cm at 10°. This is mostly explained by the fact that the ground echo does not contribute much to the final error, as it mostly behaves like a high frequency error.

We can also see in figure 31 that the standard deviation of the smoothed code tracking error is smaller for samples taken when altitude is larger than 500 ft than for samples taken even when the aircraft is on the ground. This can be explained by the fact that the GPS L1 ground echo has an increasing influence on the tracking error when the aircraft altitude is decreasing for a narrow bandwidth wide chip spacing GPS L1 C/A receiver.

Increasing the ground echo amplitude by a factor of 4 causes the tracking loops to lose lock, and therefore this increase by a factor is the maximum reasonable increase which is considered.

Another test was conducted to adapt this ground reflection power: the Markov state powers were increased in the model up to a level sufficient for the obtained sigma curve for GPS L1 C/A wide chip spacing BW2=2Mhz to match the SARPs sigma curve. This enormous increase in ground power level had no noticeable influence on the results obtained for GPS L1 C/A narrow correlator, GPS L5 GALILEO E5a/E5b and GALILEO L1 BOC(1,1). Therefore, it was decided that no adaptation of ground power echo was useful as its influence is only noticeable for GPS L1 C/A narrowband wide chip spacing receivers.

Tests were also conducted with nominal channel settings and a reduced DLL bandwidth in various configurations, that yielded exactly the same results: the ground contribution is so fast that it is wiped out by the tracking loop and smoothing.

10. CONCLUSION

A simulator using the High Resolution Aeronautical channel together with a receiver simulator has been built and used to determine statistics of the code tracking errors for GPS L1 C/A, GPS L5, GALILEO E5a, GALILEO E5b and GALILEO BOC(1,1) signals.

The major contributor to the pseudorange error is in all cases the fuselage reflection, although it has a very short delay (1.5 ns). Reducing the DLL chip spacing has a favourable impact on the reduction of the measurement error for a chip rate of 1.023 MHz, but has no impact for a chip rate of 10.23 MHz. Moreover, reducing the loops bandwidth seems useless because of the very slow variations of this fuselage echo.

As only the aircraft structure has a significant effect, the relative delay is very small and varies slowly, so a unique sigma curve can be proposed for all GNSS signals. This sigma curve is flat and can be assumed to be a constant standard deviation of 7 cm for any elevation.

We have noticed that the computed sigma is smaller than SARPs curve for all the simulations when using the High Resolution Aeronautical channel model with its default settings. For GPS L1 C/A code, this deviation is assumed to be due to the small effect of the ground reflection power level, representative of the Graz airport approach.

The validity of this ground echo parameter has been investigated. Several options were considered, and it was finally determined that when the ground echo characteristics are set to match the L1 C/A SARPs error curve for wide chip spacing receivers, the observed error sigma for narrow correlator receivers, high chip rate signals and BOC(1,1) signal again converges to the flat 7cm curve.

It is however useful to note that the ground echo characteristics has no influence on GPS L5, GALILEO E5a, GALILEO E5b signals because of its very large relative delay compared to the 10.23 MHz chip length.

ACKNOWLEDGMENTS

The authors want to acknowledge the help of all the people that supported or participated to the investigations.

Note: ANASTASIA Project (AIP4-CT-2005-516128) receives research funding from the European Community's 6th framework Programme (DG research).

REFERENCES

[Booth et al., 2000], J. Booth, T. Murphy, B. Clark, F. Liu, "Validation of the Airframe Multipath Error Allocation for Local Area Differential GPS", Proceeding of the IAIN/ION Meeting, June 2000

[Murphy and Booth, 1999], T. Murphy; J. Booth: "GBAS SARPs Review and Validation of Airborne Multipath Requirements", GNSSP WG B Toulouse 10/99 WP43

[Murphy and Booth, 2000], T. Murphy; J. Booth: "GBAS SARPs Review and Validation of Airborne Multipath Requirements", (Sections B.3.6.5.4.1 and B.3.6.8.2.1)", GNSSP WG B Canberra Jan 2000

[Murphy et al., 2005a], T. Murphy, M. Harris, J. Booth, P. Geren, T. Pankaskie, B. Clark, J. Burns, T. Urda, "Results from the Program for the Investigation of Airborne Multipath Errors", Proceedings of the ION National Technical Meeting Jan 2005

[Murphy et al., 2005b], T. Murphy, M. Harris, P. Geren, T. Pankaskie, B. Clark, J. Burns, "More Results from the Investigation of Airborne Multipath Errors", Proceedings of the ION GNSS 2005

[Steingass et al., 2004], A. Steingass, A. Lehner, F. Pérez Fontán, E. Kubista, M. Jesús Martín and B. Arbesser-Rastburg, "The High Resolution Aeronautical Multipath Navigation Channel", proceedings of ION GPS 2004.